Computational Nanomechanics of Carbon Nanotubes and Composites

Deepak Srivastava,[a*] Chenyu Wei[a,b] and Kyeongjae Cho[b*]
a: Computational Nanotechnology, NASA Ames Research Center,
Moffett Field, CA 94035-1000
b: Department of Mechanical Engineering, Stanford University, Stanford, CA 93045

Abstract: Nanomechanics of individual Carbon and Boron-Nitride nanotubes and their application as reinforcing fibers in polymer composites has been reviewed with interplay of theoretical modeling, computer simulations and experimental observations. The emphasis in this work is on elucidating the multi-length scales of the problems involved, and of different simulation techniques that are needed to address specific characteristics of individual nanotubes and nanotube polymer-matrix interfaces. Classical molecular dynamics simulations are shown to be sufficient to describe the generic behavior such as strength and stiffness modulus but are inadequate to describe elastic limit and nature of plastic buckling at large strength. Quantum molecular dynamics simulations are shown to bring out explicit atomic nature dependent behavior of these nanoscale materials objects that are not accessible either via continuum mechanics based descriptions or through classical molecular dynamics based simulations. As examples, we discus local plastic collapse of carbon nanotubes under axial compression and anisotropic plastic buckling of Boron-Nitride nanotubes. Dependence of the yield strain on the strain rate is addressed through temperature dependent simulations, a transition-state-theory based model of the strain as a function of strain rate and simulation temperature is presented, and in all cases extensive comparisons are made with experimental observations. Mechanical properties of nanotube-polymer composite materials are simulated with diverse nanotube-polymer interface structures (with van der Waals interaction). The atomistic mechanisms of the interface toughening for optimal load transfer through recycling, high-thermal expansion and diffusion coefficient composite formation above glass transition temperature, and enhancement of Young's modulus on addition of nanotubes to polymer are discussed and compared with experimental observations.

* Authors to whom correspondence should be addressed.

Index:

1. Introduction

Since the discovery of multi-wall carbon nanotubes in 1991 by Iijima, (Iijima 1991) [1], and subsequent synthesis of single-wall carbon nanotubes by others (Iijima [2] and Bethune [3]) there are numerous experimental and theoretical studies of their electronic, chemical, and mechanical properties. Chemical stability, diverse electronic properties (ranging from 1eV band gap semiconductors to metals), and predicted extreme strength of the nanotubes have placed them as fundamental building blocks in the rapidly growing field of nanotechnology. Diverse nanoscale device concepts have been proposed to develop nanoscale electronic devices, chemical sensors, and also high strength nanotube composite materials with sensing and actuating capacity. To realize the proposed devices and materials concepts, it is crucial to gain detailed understanding on the fundamental limits of nanotubes' diverse properties. Atomistic simulations are very promising approach to achieve this goal since one can investigate a large range of possibilities which are often very difficulty to access through experimental studies. The insights and detailed mechanistic understanding provides valuable guiding principles to optimize and develop novel nanoscale device and materials concepts.

In this review chapter, we focus our discussion on the mechanical properties of carbon nanotubes in the context of high strength nanotube composite materials. For the purpose of high strength nanomaterials application of nanotubes, it is crucial to gain detailed understanding on nanotubes' intrinsic mechanical properties as well as their interaction with polymer matrix in nanotube-polymer composite materials. First, we have examined the elastic and failure properties of nanotube to understand their fundamental strength and stiffness behavior. Initial atomistic simulations of nanotube mechanics have predicted unusually large Young's modulus (of up to 5TPa or 5 times larger than the modulus of diamond) and elastic limits (of up to 20-30% strain before failure). These predictions immediately raised the intriguing possibility of applying the nanotubes as super strong reinforcing fibers with orders of magnitude higher strength and stiffness than any known material. Subsequently, more accurate simulations employing tight-binding molecular dynamics methods and *ab-initio* density functional total energy calculations involving realistic strain rate, temperature dependence, and nanotube sizes have provided more realistic values of 1TPa as Young's modulus and 5-10% elastic limit of the strain before failure. These values predict 50 GPa as the nanotube strength in good agreement with recent experimental observations. Second, we have examined the mechanical properties of nanotube-polymer composite materials to understand the mechanisms of mechanical load transfer between a polymer matrix and embedded nanotubes. This research area is rapidly moving forward with exciting possibilities of designing and developing very small structures (e.g., MEMS devices) with tailored mechanical properties. Near term practical applications of nanotubes are expected to emerge from the composite materials as they do not require a precise control of nanotube positioning for device applications. For the future development of smart nanotube-polymer composite materials computational modeling will play a catalytic role in facilitating and accelerating the design and fabrication of composite materials with sensing, actuation, and self-healing capabilities.

2. Carbon Nanotubes: Structure and Properties

A single-wall carbon nanotube (SWNT) is best described as a rolled-up tubular shell of graphene sheet [Fig.1a], which is made of benzene-type hexagonal rings made of carbon atoms. [4, 5] The body of the tubular shell is thus mainly made of hexagonal rings (in a sheet) of carbon atoms, where as the ends are capped by (half-)dome shaped half-fullerene molecule. The natural curvature in the side-walls is due to the rolling of the sheet into the tubular structure, whereas the curvature in the end caps is due to the presence of topological (pentagonal ring) defects in the otherwise hexagonal structure of the underlying lattice. The role of the pentagonal ring defect is to give a positive (convex) curvature to the surface, which helps in closing of the tube at the two ends. A multi-wall nanotube (MWNT) is a rolled-up stack of graphene sheets into concentric SWNTs, with the ends again either capped by half-fullerenes or kept open. A nomenclature (n,m) used to identify each single-wall nanotube, in the literature, refers to integer indices of two graphene unit lattice vectors corresponding to the chiral vector of a nanotube. [4] Chiral vectors determine the directions along which the graphene sheets are rolled to form tubular shell structures and perpendicular to the tube axis vectors as explained in the Ref. 4. The nanotubes of type (n,n), as shown in Figure 1b, are commonly called armchair nanotubes because of the _/_/ shape, perpendicular to the tube axis, and have a symmetry along the axis with a short unit cell (0.25 nm) that can be repeated to make the entire section of a long nanotube. Another nanotubes of type (n, 0) are known as zigzag nanotubes (Fig 1c) because of the /\/\ shape perpendicular to the axis and also have a short unit cell (0.43 nm) along the axis. All the remaining nanotubes are know as chiral or helical nanotubes and have longer unit cell sizes along the tube axis. Details of the symmetry properties of the nanotubes of different chiralities are explained in detail in Refs. 4 and 5.

The single and multi-wall nanotubes are interesting nanoscale materials for the following four reasons:

- Single and multi-wall nanotubes have very good elasto-mechanical properties because the two dimensional arrangement of carbon atoms in a graphene sheet allows large out-of-plane distortions, while the strength of carbon-carbon in-plane bonds keeps the graphene sheet exceptionally strong against any in-plane distortion or fracture. These structural and materials characteristics of nanotubes point towards their possible use in making next generation of extremely lightweight but highly elastic and very strong composite materials.
- A single-wall nanotube can be either metallic or semiconducting, depending on its chiral vector (n,m), where n and m are two integers. The rule is that when the difference n-m is a multiple of three a metallic nanotube is obtained. If the difference is not a multiple of three, a semiconducting nanotube is obtained. In addition it is also possible to connect nanotubes with different chiralities creating nanotube hetero-junctions, which can form a variety of nanoscale molecular electronic device components.
- Nanotubes, by structure, are high aspect-ratio objects with good electronic and mechanical properties. Consequently the applications of nanotubes in field-emission displays, or scanning probe microscopic tips for metrological purposes have started to materialize even in the commercial sector.

- Since nanotubes are hollow, tubular, caged molecules they have been proposed as lightweight large surface area packing material for gas-storage and hydrocarbon fuel storage devices, gas or liquid filtration devices, as well as nanoscale containers for molecular drug-delivery and casting structures for making nanowires and nanocapsulates.

A broad interest in nanotubes derives from the possibilities of a variety of applications in all of the above four technologically interesting areas. In this review we mainly focus on the exceptionally stiff and strong mechanical properties that can be used for making future generation of lightweight structural composite materials. The other three interesting electrical, surface area, and aspect-ratio characteristics could be used to impart specific functional behavior to the thus prepared composite materials.

3. Simulation Techniques:

In the earlier days the structural, mechanical and thermal properties of interacting, bulk condensed matter systems were studied with analytical approximation methods for infinite systems. Numerical computer simulations of the finite sample systems have become the more common recently because powerful computers to simulate nano-scale systems in full complexity are readily available. Atomistic molecular dynamics (MD) refers most commonly to the situation where the motion of atoms or molecules is treated in approximate finite difference equations of Newtonian mechanics. Except when dealing with very light atoms and very low temperatures, the use of classical MD method is well justified.

The MD code for carbon based systems involve analytic many-body force field functions such Tersoff-Brenner [6] potentials for C-C and C-H interactions. [7] The Tersoff-Brenner potential is specially suited for carbon based systems, such as diamond, graphite, fullerenes and nanotubes, and has been used in a wide variety of scenarios with results in agreement with experimental observations. Currently, there are no universal analytic many-body force field function that works for all materials and in all scenarios. In its global structure a general MD code typically implements an algorithm to find a numerical solution of a set of coupled first-order ordinary differential equations given by the Hamiltonian formulation of Newton's second law. [8] The equations of motion are numerically integrated forward in finite time steps using a predictor-corrector method. A major distinguishing feature of the Tersoff-Brenner potential for carbon based systems is that short-range bonded interactions are reactive so that chemical bonds can form and break during the course of a simulation. Therefore, compared to some other molecular dynamics codes, the neighbor list describing the environment of each atom includes only a few atoms and needs to be updated more frequently. The computational cost of the many-body bonded interactions is relatively high compared to the cost of similar methods with non-reactive interactions with simpler functional forms. As a result, the overall computational costs of both short-range interactions and long-range, non-bonding van der Waals (Lennard-Jones 6-12) interactions are roughly comparable. For large scale atomistic modeling (10^5-10^8 atoms), multiple processors are used for MD simulations, and the MD codes are generally parallelized. [9]

In recent years several more accurate quantum molecular dynamics schemes have been developed in which the forces between atoms are computed at each time step via quantum mechanical calculations within the Born-Oppenheimer approximation. The dynamic motion for ionic positions are still governed by Newtonian or Hamiltonian mechanics, and described by molecular dynamics. In the intermediate regimes, for up to few thousand atoms, the tight-binding [10] molecular dynamics (TBMD) approach provides very good accuracy for both structural and mechanical characteristics. The computational efficiency of the tight-binding method derives from the fact that the quantum Hamiltonian of the system can be parameterized. Furthermore, the electronic structure information can be easily extracted from the tight-binding Hamiltonian, which in addition also contains the effects of angular forces in a natural way. In a generalized *non-orthogonal* tight-binding molecular dynamics (TBMD) scheme Menon and Subbaswami have used minimal number of adjustable parameters to develop a transferable scheme applicable to clusters as well as bulk systems containing Si, C, B, N and H. [11,12] The main advantage of this approach is that it can be used to find an energy minimized structure of a nanoscale system under consideration without symmetry constraints.

Additionally, *ab-initio* or first principles method is a simulation method to solve complex quantum many-body Schroedinger equation using numerical algorithms.[13] *Ab-initio* method provides more accurate description of quantum mechanical behavior of materials properties even though the system size is currently limited to only about few hundred atoms. Current *ab-initio* simulation methods are based on a rigorous mathematical foundation of the density functional theory (DFT). [14] [15] This is derived from the fact that the ground state total electronic energy is a functional of the density of the system. The ground state density is expressed by single electron wave functions, and these single electrons are governed by self-consistent Schroedinger equation with unknown exchange-correlation potential. The exchange-correlation potential is approximated by the local density approximation (LDA). For practical applications the DFT-LDA method has been implemented with a pseudopotential approximation and a plane wave (PW) basis expansion of single electron wave functions.[13] These approximations reduce the electronic structure problem as a self-consistent matrix diagonalization problem. One of the popular DFT simulation programs is Vienna Ab intio Simulation Package (VASP), which is available through a license agreement. (VASP) [16]

For computational nanomechanics of nanotubes all the three simulation methods can be used in a complementary manner to improve the computational accuracy and efficiency. Based on experimental observations or theoretical dynamic and structure simulations, the atomic structure of a nanosystem can first be investigated. After the nanoscale system configurations have been finalized, the functional behaviors of the system are investigated through static *ab-initio* electronic energy minimization schemes. We have covered this in detail in a recent review article focusing exclusively on computational nanotechnology. [17]

In the following we describe nanomechanics of nanotubes and nanotube-polymer composites, and compare the simulation results, where ever possible, with experimental observations.

4. Modulus of Nanotubes:

The modulus of the nanotube is a measure of the strength and stiffness against small axial stretching and tensile strains as well as non-axial bending and torsion strains

on the nantubes. The simulation results mainly pertain to the strength and stiffness of SWNTs, where as most of the experimental observations available so far are either on MWNTs or ropes/bundles of nanotubes. For axial strains, SWNTs are expected to be stiffer than the MWNTs because of smaller radii of curvature and relatively defect free structure. For non-axial strains such as bending and torsion, the MWNTs are expected to be stiffer than the SWNTs. In this section, the axial, bending and torsion moduli of SWNTs are described and compared with experimental observations known so far.

4a. Young's Modulus for Axial Deformations

As described above, single-wall carbon nanotubes have tubular structure that can be conceptualized by taking a graphene sheet, made of C atoms, and rolling into long tubular shape. Contributions to the strength and stiffness of SWNTs come mainly from the strength of graphene in-plane covalent C-C bonds. It is expected that modulus, strength and stiffness of SWNTs should be comparable to the in-plane modulus and strength of graphene sheet. In the tubular shape, however, the elastic strain energies are effected by the by the intrinsic curvature of C-C bonds. Robertson et al (1992) [18] have found, (using both Tersoff potential and Tersoff-Brenner potential), that the elastic energy of a SWNT scales as $\frac{1}{R^2}$, where R is the radius of the tube. This is similar to as deduced from the continuum elastic theory. [19] The elastic energy of CNTs responding to a tensile stress in their study suggested that SWNTs are very strong materials and that the strength is mainly due to the strong C-C sp^2 bonds on the nanotube. The Young's modulus of a SWNT is defined as $Y = \frac{1}{V}\frac{\partial^2 E}{\partial \varepsilon^2}$, where E is the strain energy and V is the volume of the nanotube. Using an empirical force constant model, J.P. Lu (1997) [20] found that the Young's modulus of a SWNT is around 970GPa, which is close to that of a graphite plane, and is independent of tube diameter and chirality. A. Rubio et al (1998) [21] used a better description for interatomic forces through a non-orthogonal tight-binding method and found the Young's modulus to be around 1.2TPa, which is better than that of graphite, and is also slightly dependent on the tube size especially for small diameter nanotubes (D <1.2nm). High surface curvature for small diameter nanotubes tends to decrease the Young's modulus. In both of these studies the thickness of the nanotube wall was assumed to be 0.34nm and the computed results are within the range of experimental observations.

Young's moduli of variety of non-carbon nanotubes as a function of tube diameter have been calculated and shown in figures 2 and 3. Initial computational studies, [22] using the same Tersoff-Brenner potential, however, reported the values of Young's modulus to be as high as 5.5TPa. This was mainly due to a very small value of wall thickness (h~0.06nm) used in these studies. It has been suggested that by investigating the value $\partial^2 E/\partial \varepsilon^2$ instead of Young's modulus, the ambiguity of thickness of CNT wall can be avoided. Using the density functional theory (with pseudopotentials) Rubio et al have found that the stiffness of SWNTs is close to that of in-plane stiffness of graphite, and SWNTs made of carbon are strongest as compared with other non-carbon, such as boron-nitride (BN) or BCxNy, nanotubes known so far. [23] Using a non-orthogonal tight-binding molecular dynamics method and DFT method, we recently carried [24] out axial compression of single-wall C and BN nanotubes and have found the Young's modulus to be about 1.2 TPa, and that the modulus of a similar BN nanotube is about 80% of that of the carbon nanotube. These results are in qualitative and quantitative agreement with Rubio's DFT results and the general experimental observations known so far. The Young's modulus of MWNTs and ropes of SWNTs have also been estimated in Rubio et al's studies and shown in Fig. 3.

4b. Bending Stiffness and Modulus

Besides axial strains discussed above, SWNTs have also been subjected to bending and torsional strains. The bending stiffness of a SWNT is defined as $\frac{1}{L}\frac{d^2 E}{dC^2}$, where E is the total strain energy, L is the length, and C is the curvature of the bent nanotube, which is related with the bending angle θ as $C = \frac{\theta}{L}$. From the elastic theory of bending of beams, the strain energy of a bent nanotube can be expressed as $E = 0.5 Y h L \int t^2 C^2 dl$, where Y the Young's modulus of the SWNT, and h is the thickness of the wall. [25] The integral is taken around the circumference of the nanotube, and t is distance of atoms from the central line (or the bent axis) of the tube. From this expression, the bending stiffness K is found to be equal to $Yh(\pi r^3)$, i.e., and scales as cubic of the radius of the tube. Results from molecular dynamics simulation with Tersoff-Brenner potential show that stiffness K scales as $R^{2.93}$ (Figure 4), which is in good agreement with scaling predicted by the continuum elastic theory. The corresponding bending Young's modulus (Y_B) of SWNTs with varied diameters can be calculated from above equation. For a small diameter SWNT Y_B is found to be about 0.9 TPa, smaller than the stretching Young's modulus calculated from the tight-binding method or first principle theory. The computed smaller value is also similar to what Robertson et al (1992) [18] showed in their study of the elastic energy of SWNTs. The qualitative agreement is rather good. An additional feature is that the bending Young's modulus decreases with the increase in tube diameter. This is mainly due to more favorable out-of-plane displacements of carbon atoms on a larger diameter tube, resulting in flattening of the tube in the middle section.

Poncharal et al (2000) [26] have experimentally studied the bending Young's modulus of MWNTs (diameter >10nm) using electrically induced force and have found that the bending Young's modulus is decreased sharply with the increase in tube diameter, (Figure 5a) which they have attributed to the wave-like distortion of the MWNT as shown in Figure 5b.

At a large bending angle, SWNTs can buckle sideways similarly to a macroscopic rod, at which non-uniform strain is induced. Shown in Figure 6a and 6b are the images from high-resolution electron microscope [27] of the buckling of bent SWNT and MWCNT. Such buckling at large bending angle is closely related with buckling of SWNT under axial compression stress, which will be discussed later.

4c. Torsion stiffness and modulus

The torsion stiffness of a CNT is defined as $K = \frac{1}{L}\frac{d^2E}{d\theta^2}$, where E is the total strain energy and θ is the torsion angle. The shear strain is related with torsion angle as $\varepsilon = \frac{R\theta}{L}$, where R is the radius of tube and L is its length. From continuum elastic theory, the total strain energy of a cylinder can be written as $E = \frac{1}{2}G * \iiint \varepsilon^2 dV$, where G is shear modulus of the tube. The torsion stiffness thus is related with G as $K = \frac{1}{L}\frac{d^2E}{d\theta^2} = G(2\pi h)\frac{R^3}{L^2}$, where h is the thickness of the wall of the nanotube. In Figure 7, we show our recently computed values of the torsion stiffness of several armchair and zigzag carbon nanotubes using Tersoff-Brenner potential. The dependence of the torsion stiffness on the radius of tube is found to be as $K \propto R^{3.01}$ (for tube diameter >0.8nm). This is in excellent agreement with the prediction of cubic dependence from the continuum elastic theory.

The shear modulus of CNTs found to be around 0.3TPa and is not strongly dependent on diameters (for D>0.8nm). This value is smaller than that of about 0.45Tpa in Lu (1997)'s study, [20] calculated with an empirical force constant model. For small diameter tube. such as a (5,5) nanotube, the shear modulus derivates away from the continuum elastic theory description.

4d. Experimental status: modulus of Carbon nanotubes

The high strength of carbon nanotubes has been verified by several experiments. M. Treacy et al (1996) [28] studied the Young's modulus of MWNTs by measuring the thermal vibrations, and Y was found to be about (1.8±1.4) TPa. Later studies by Wong et al (1997) [29] on MWCNT found the Young's modulus to be about (1.28±0.59) TPa by measuring the restoring force of bent nanotubes. A. Krishnan et al (1998) [30] have conducted study on the stiffness of single-walled nanotubes and have found an average Young's modulus to be about 1.25Tpa. This is close to the experimental results obtained by Salvetat et al (1999), [31] where Y is found to be about 1TPa.

5. Plastic Deformation and Yielding of Nanotubes

Nanotubes under large strain go through two kinds of structural changes. First, early simulations by Yakobson et al (1996) [22] showed that under axial compression, nanotubes exhibit structural instabilities resulting in sideways buckling but the deformed structure remains within elastic limit. Second, under large strains, bonding rearrangements or transitions occur giving rise to permanent damage, plastic deformation, or yielding of nanotubes. In this section, we discus plastic deformation and failure under large axial compression and tensile strains. Critical dependence of the yielding of nanotubes on the applied strain-rate and the kinetic temperature of the simulation is also discussed through a model that shows that nanotubes may typically yield with in 5-10% tensile strain at room temperature. This finding is in good agreement with the experimental observations on the breaking and yielding of MWNTs and the ropes or bundles of SWNTs.

5a. Plastic deformation under compressive strain

Yakobson et al (1996) [22] found that SWNTs form non-uniform "fins" like structure under large compressive strain (Fig 8), The sideways displacement or buckling of tubes occur, for larger strain, and contributes towards the relief of strain energy from the "fins" like structure but the tubes remain super-elastic for more than 20% compressive strains. Experiments have observed sideways buckling feature in compressed multi-wall nanotubes in polymer composite materials. [32] Another mode of plastic deformation of compressed thin nanotubes is also observed in the same experiments, [32] i.e., the tubes remain essentially straight but the structure locally collapses as shown in figure 9. Srivastava et al (1999) [33] used tight-binding molecular dynamics method, and have found that with in Euler buckling length limitation, an (8,0) carbon nanotube locally collapses at 12% compressive strain. The local plastic collapse is due to a graphitic (sp^2) to diamond like (sp^3) bonding transition at the location of the collapse and the release of excess strain in the remaining uncollapsed section. The released strain in the uncollapsed section drives the local collapse with a compressive pressure as high as 150 GPa at the location of the collapse (Figure 10).

Srivastava et al (2001) [24] have also studied the influence of changes in the chemical nature on the nanomechanics and the plasticity of nanotubes. For example, this is done by considering the structure, stiffness and plasticity of boron-nitride (BN) nanotubes. The results for the Young's modulus of BN nanotubes are discussed above. It turns out that BN nanotubes are only slightly less stiff (80-90%) as compared to their carbon equivalent. The tight-binding MD and *ab-initio* total energy simulations further show that, due to BN bond rotation effect, (BN) nanotubes show anisotropic response to axial strains. For example, Fig. 11 shows spontaneous anisotropic plastic collapse of a BN nanotube that has been compressed at both ends, but the strain release is shown to be more favorable towards nitride atoms in the rotated BN bonds. This results in the anisotropic buckling of the tube towards one end when uniformly compressed at both ends.

5b. Plastic deformation under tensile strain

For the case of tensile strain, Nardelli et al (1998) [34] have studied the formation of Stone-Wales (SW) bond rotation induced defects as causing the plastic deformation of nanotubes. This mechanism is explained by formation of heptagon-pentagon pair (5775) defects in the wall of nanotubes. (Fig. 12) The formation energy of such defects is decreased with the applied strain, and is also dependent on the diameter and chirality of the nanotube under consideration. At high temperatures, plastic flow of the thus formed defects occurs, and that can even change the chirality of the nanotube (Fig. 13). On further stretch, the plastic flow and increased formation of more such defects continue until necking and breaking of the nanotube occurs. Zhang et al (1999) [35] have also studied the plastic deformations of SWNTs induced by the Stone-Wales dislocations under tensile strain, and they have found that the SW defects can release the strain energy

in the system. Zhang et al note that SW defects form more favorably on an armchair nanotube than on a zigzag nanotube because the rotation of the C-C bond can compensate more tensile strain along the axis in the former case.

5c. Strain-rate and temperature dependence of yielding of nanotubes

In all the simulations and discussions, so far, no dependence of the failure or yielding of nanotubes on the rate of the applied strain and the temperature of the system has been mentioned. This is because all of the above results were either obtained with the *ab-initio or* tight binding static total energy calculations or with MD simulations at much higher strain rates (than ever possible in experiments) where barriers to collapse would be artificially higher. In reality, it is expected that barrier to collapse and yielding strain at experimentally realizable strain rates and at room temperatures maybe lower than the simulation values reported so far. The yielding failure of SWNTs in different scenarios depends on the formation of defects discussed above. Classical MD simulations report values [36] as high as 30% yielding strain under tensile stretch and above 20% under compression. [22] Due to the limitations in the time scales of the phenomenon that can be simulated with MD, the nanotubes were typically strained at 1/ns at 300-600K. The experiments so far suggest much lower yielding strains for nanotubes. Walters et al (1999) [37] have studied the SWNT rope under large tensile strain and observed the maximum strain to be 5.8±0.9% before yielding occurs. Yu et al (2000) [38] have found similar breaking strain (5.3% or lower) for different SWNT rope samples (Figure 14a). Similar measurements on MWNTs by Yu et al (2000) [39] show breaking strain to be about 12% or lower (the lowest one is 2% in their experiments) (Figure 14b). The reported lower yielding strains in experiments could be partly due to defected tubes in the SWNT ropes or could be due to much (orders of magnitude) lower rates at which strain can be applied in experiments.

The breaking, collapse or yielding of the nanotubes is clearly a temperature and strain rate dependent phenomenon, and a model needs to be developed to relate the reported much higher yielding strain from simulation studies to the so far observed lower yielding strain in experiments. We (Wei et. al, 2002) [40] have recently developed a transition-state theory based model for deducing strain rate and temperature dependence of the yielding strain as simulated in MD studies. According to Arrhenius formula the transition time for a system to go from pre-yielding state to another (post yielding) state is dependent on the temperatures as $t = \frac{1}{\nu} e^{E_v / KT}$, where E_v is the activation energy and ν is the effective vibration frequency or attempts for the transition. For a system with strain ε, the activation barrier is lowered as $E_v = E_v^{\,0} - kV\varepsilon$, where k is force constant, and V is the activation volume. At higher temperatures, therefore, a system has larger kinetic energy to overcome the barrier between the pre-yielding and post-yielding states and the transition time is shortened. Similarly, the lower strain rate at each step allows the system to find an alternative minimum energy path and thus again lowering the effective barrier height separating the pre- and post-yielding states.

For example, yielding strain of a 6nm long (10,0) SWNT at several temperature and strain rate varying between $10^{-3}/ps$ to $10^{-5}/ps$ is shown in Figure 15. Yielding strains are found to be 15% at low temperature and 5% at high temperature at about $10^{-5}/ps$ strain rate. Stone-Wales rotations are found to first appear before necking, resulting in heptagon and pentagon pairs, which provide the cores for formations of larger rings, and further resulting in the breakings of the nanotubes (Figure 16). Detailed analysis shows that [40] the complex dependence on the temperature and the strain rate with transition state theory (TST) can be expressed as $\varepsilon_Y = \frac{\overline{E}_v}{KT} + \frac{KT}{YV} \ln(\frac{N\&\&}{n_{site}\&\&})$, where $\overline{E}_v$ is the averaged barrier for the yielding initiating defect, N is the number of processes involved in the breaking of the tube, Y is Young's modulus, and n_{site} is number of sites available for yielding, which is dependent on the structural details, and $\&\&$ is a constant related with vibration frequency of C-C bonds. For a more realistic strain rate such as 1%/hour, the yielding strain of the 6nm long (10,0) CNT can be estimated to be around 11%. A longer CNT will have a smaller yielding strain, as more sites are available for defects. The difference between the yielding strain of a nanometer long CNT and of a micron meter long CNT can be around 2% according to the above expression for the yielding strain. [40] The advantage of such a model is that one could directly compute the activation energy for yielding defect formation and get the yielding strain from the developed model. Within error bars on the known activation energies computed so far, our model is in very good agreement with experimental observations.

Under compressive strain, on the other hand as described above, Srivastava et al (1999) [33] showed that CNT collapses with the graphitic to diamond like bonding transition at the location of the collapse. Another observation is the formation of non-uniform "fins" like structure by Yakobson et al (1996) [22] that gives to side-ways Euler buckling of the tube and no diamond-like bonds or defects would form within the structure. Recent MD studies at finite temperatures (Wei et. al., 2001) [41] give different results. Using the same Tersoff-Brenner potential in MD studies Wei et al (2001) [41] show that, with thermal activation, nanotubes under compressive strain can form both diamond like bonds and SW like dislocation defects at high temperatures (Figure 17). Similar analysis of nanotubes under compressive strain, therefore is more complicated and currently underway because sideways buckling can occur before tube yields with SW dislocation or diamond like defect formation.

6. Structure and Mechanics of Nanotube Composites

As discussed above, the strong in-plane graphitic C-C bonds make defect free SWNTs and MWNTs exceptionally strong and stiff against axial strains and very flexible against non-axial strains. Additionally nanotubes also have very good electrical and thermal conduction capabilities. Many applications, therefore, are proposed for nanotubes as additive fibers in light weight multi-functional composite materials. Several recent experiments on the preparation and characterization of nanotube-polymer composite materials have also appeared [42-44] These measurements suggest modest enhancement in strength characteristics of CNT-embedded polymer matrices as compared to the bare polymer matrices. Vigolo et al (2000) [42] have been able to condense nanotubes in the

flow of a polymer solution to form nanotube ribbons as well. These can be strongly bent without breaking and have Young's modulus that is an order of magnitude larger than that of the bucky paper. In the following we discuss structural, thermal and mechanical implications of adding SWNTs to polyethylene polymer samples.

6a. Structural and thermal behavior of nanotube-polyethylene composite

Thermal properties of polymeric materials are important from both processing and applications perspective. As a function of temperature, polymeric materials go through structural transformation from solid to rubber to liquid states. Many intermediate processing steps are done in the liquid or rubber-like state before the materials is cooled down to below glass transition temperature for the finally needed structural application. Besides the melting process at high temperature T_m, like other solid materials, the structural and dynamic behavior of polymeric material above and below glass transition temperature T_g is important to investigate. Below T_g the conformations of polymer chains are frozen, when the polymer is in a solid glassy state, and in between T_g and T_m polymers are in a rubber like state with viscous behavior. Preliminary experimental and simulation studies on the thermal properties of individual nanotubes show very high thermal conductivity of SWNTs. [45] It is expected, therefore, that nanotube reinforcement in polymeric materials may also significantly change the thermal and structural properties as well.

Atomistic MD simulation studies of the thermal and structural properties of nanotube-polyethylene composite have been attempted recently. [46] Polyethylene is a linear chain molecule with CH_2 as the repeating unit in the chain. The density as a function of temperature for a pure polyethylene system (a short chain system with 10 repeating unit in each polymer with 50 polyethylene chains in the simulation sample) and a nanotube-polyethylene composite system with about 8% volume ratio capped nanotubes in the mixture is shown in Fig. 18. Both systems show discontinuity in the slope of the density-temperature curve. The discontinuities represent glass transition temperatures in the two cases. Two features are apparent from in the figure. First, the glass transition temperature of the composite system has increased to higher value than the pure polyethylene system. Second, above glass transition temperature in both the cases, the density as a function of temperature in the composite case decreases at much faster rate than the decrease in the pure polyethylene system case. This means that the volume thermal expansion coefficient of the composite has increased to a larger value above glass transition temperature. The volume thermal expansion coefficient for the composite system above glass transition temperature is found to be $12 \bullet 10^{-4} K^{-1}$, which is 40% larger than that of the pure polyethylene system above T_g. The increase in the thermal expansion coefficient due to mixing of SWNTs in the polymer sample is attributed to the increased excluded volume due to thermal motions of the nanotubes in the sample. In the same simulations we also found that, above glass transition temperature, the self-diffusion coefficient of the polymer molecules in the composite increases as much as 30% above their pure polyethylene sample values. The increase in the diffusion coefficient is larger along the axis of the added nanotube fibers and could help during the processing steps due to better flow of the material above glass transition temperature.

b. Mechanical behavior of nanotube-polyethylene composite

Using fibers to improve the mechanical performance of a composite material is a very common practice and the related technology has been commercialized for quite some time. Commonly used fibers are glass, carbon black, or other ceramics. These not only can add structural strength to the material but also can add desired functionality in thermal and electrical behavior. The structural strength characteristics of such composite materials depend on the mechanical load transfer from the matrix to the fiber and the yielding of the coupling between the two. Mechanical load from matrix to the fibers in a composite is transferred through the coupling between the two. In some cases, the coupling is through chemical inter-facial bonds, which can be covalent or non-covalent in nature, while in other the coupling could be purely physical in nature through non-bonded Van der Waals (VDW) interactions. Covalently coupled matrix and fibers are strongly interacting systems while VDW coupled systems are weakly interacting systems but occur in a wide variety of cases. The aspect ratio of fiber, which is defined as L/D (L is the length of the fiber and D is the diameter), is also an important parameter for the efficiency of load transfers, because the larger surface area of the fiber is better for larger load transfer. It is expected, therefore, that the embedded fibers would reach their maximum strength under tensile load only when the aspect ratio is large. The limiting value of the aspect ratio is found related with the interfacial shear stress τ as $L/D > \sigma_{max}/2\tau$, where σ_{max} is the maximum strength of the fiber. Recent experiments on MWNTs or SWNT ropes [38-39] have reported the strength of the nanotubes to be in the range of 50GPa. With a typical value of 50MPa for the interfacial shear stress between the nanotube and the polymer matrix, the limiting value of the aspect ratio is 500:1. Therefore, for an optimum load transfer with a MWNT of 10nm diameter, the nanotube should be at least 5μm long, which is the range of the length of nanotubes typically investigated in experiments on nanotube reinforced composites.

Earlier studies of the mechanical properties of the composites with macroscopic fibers are usually based on continuum media theory. The Young's modulus of a composite is expected to be within a lower bound of $\frac{1}{Y_{comp}} = \frac{V_{fiber}}{Y_{fiber}} + \frac{V_{matrix}}{Y_{matrix}}$ and an upper bound of $Y_{comp} = V_{fiber} Y_{fiber} + V_{matrix} Y_{matrix}$, where V_{fiber} and V_{matrix} is the volume ratio of the fibers and the matrix respectively. The upper bound obeys the linear mixing rule, which is followed when the fibers are continuous and the bonding between fibers and the matrix is perfect, i.e., the embedded fibers are strained by the same amount as the matrix molecules. The lower bound is reached for the case of particulate filler composites because the aspect ratio is close to one. For a nanotube fiber composite, therefore, an upper limit can be reached if the nanotubes are long enough and the bonding with the matrix is perfect. Additionally, short nanotubes, with Poisson ratio of about 0.1 to 0.2, are much harder material as compared to the polymer molecules with Poisson ratio of about 0.44. Therefore, as a nanotube containing polymer matrix is stretched under tensile strain there is a resistance to the compression pressure perpendicularly to the axis of the

tube. For the short but hard nanotubes and soft polymer matrix mixture, this provides additional mechanism of load transfer that is not possible in other systems.

An MD simulation of the mechanical properties of a composite sample was recently performed with short nanotubes embedded in short-chained polyethylene system at 50K, a temperature below glass transition temperature. The coupling at the interface was through non-bonded Van der Waals interactions. Shown in Figure 19 is the strain-stress curve for both the composite system and the pure polyethylene matrix system. The Young's modulus of the composite is found to be 1900MPa, which is about 30% larger than that of the pure polymer matrix system. This enhancement is within the upper and lower bound limits discussed above. We have found that further enhancement of the Young's modulus of the same sample can be achieved by carrying the system through repeated cycles of the loading-unloading of the tensile strain on the composite matrix. In agreement with the experimental observation, this tends to align the polymer molecules with the nanotube fibers causing a better load transfer between the two. Frankland et al (2000) [47] have studied the load transfer between polymer matrix and SWNTs, and have found that there was no permanent stress transfer for 100nm long (10,10) CNTs within polyethylene if only Ver der Waals interaction present. In the study they estimated that the interfacial stress could be 70MPa with chemical bonding between SWCNT and polymer matrix, while only 5MP for the nonbonding case.

c. Experimental status

Using nanotubes as reinforcing fibers in composite materials is still a developing field from theoretical and experimental perspectives. Several experiments regarding the mechanical properties of nanotube-polymer composite materials have been reported recently. Wagner et al (1998) [48] experimentally studied the fragmentation of MWNTs within thin polymeric films (urethane/diacrylate oligomer EBECRYL 4858) under compressive and tensile strain. They have found that nanotube-polymer interfacial shear stress τ is of the order of 500MPa, which is much larger than that of conventional fibers with polymer matrix. This has suggested the possibility of chemical bonding between the nanotubes and the polymer in their composites. The nature of the bonding, however, is not clearly known. Later Lourie et al (1998) [49] have studied the fragmentation of single-walled CNT within the epoxy resin under tensile stress. Their experiment also suggested a good bonding between the nanotube and the polymer in the sample. Schadler et al (1998) [43] have studied the mechanical properties of 5 wt. % MWNTs within epoxy matrix by measuring the Raman peak shift when the composites are under compression and or under tension. A large Raman peak shift is observed for the case of compression, while the shift in the case of tension is not significant. The tensile modulus of the composites is found to enhance much less as compared to the enhancement in the compression modulus of the similar system. Schadler et al have attributed the differences, between the tensile and compression strain cases, to the sliding of inner shells of the MWNTs when a tensile stress was applied. In cases of SWNT polymer composites, the possible sliding of individual tubes in the SWCNT rope, which is bonded by Van der Waals forces, may also reduce the efficiency of load transfer. It is suggested that for the SWNT rope case, interlocking using polymer molecules might bond SWCNT rope more strongly. Andrews at al (1999) [44] have also studied the composites of 5 wt. % of SWNT embedded in petroleum pitch matrix and their measurements show an enhancement of the Young's modulus of the composite under tensile stress. Qian et al (2000)'s measurement of a 1 wt. % MWNT-polystyrene composite under tensile stress also show a 36% increase of Young's modulus compared with the pure polymer system.[50] The possible sliding of inner shells in MWCT and of individual tubes in a SWNT rope was not discussed in these later two studies. There are at present no experiments available on SWNT-polymer composite to compare above our simulated values with the experimental observations. However, if it is assumed that polymer matrix essentially bonds only to the outer shell of a MWNT embedded in a matrix, the above simulation findings could be qualitatively compared with experiments. This issue needs to be considered in more detail before any direct comparison is made between theory/simulations and experimental observations.

7. Comments:

Nanomechanics of single-wall carbon nanotubes are discussed from a perspective of their prospective applications in carbon nantube reinforced composite materials. It is clear that for single-wall carbon nanotubes, a general convergence has started to emerge between the simulated Young's modulus values and the values observed in experiments so far. The Young's modulus is slightly larger than 1 TPa, tubes can withstand about 5-10% axial strains before yielding, and these corresponds to a stress of about 50 GPa before nantubes yield. Bending and torsional modulus and stiffness have also been computed but no comparison with experiments is available so far. A real progress is made in coming up with a transition state theory based model of the yielding of SWNTs under tensile stress. The yielding is identified as a barrier dependent transition between the pre- and post-yielding configurations. The model, with in the error bars of the computed activation barrier, correctly predicts that under tensile strain at realistic (experimentally realizable) strain rates, yield occurs at about 5-10% applied strain, but not at high yielding strains of 20-30% as was predicted in the earlier MD simulations. Preliminary results of the structural, thermal and mechanical characterization of nanotube polymer composites have been obtained and show that important characteristics such as thermal expansion and diffusion coefficients from the processing and applications perspective can be simulated for computational design of nanotube composite materials. These simulations illustrate the large potential of computational nanotechnology based investigations. For larger system sizes, and realistic interface between nantubes and polymer, the simulation techniques and underlying multi-scale simulations and modeling algorithms need to be developed and improved significantly before high fidelity simulations can be attempted in the near future.

Acknowledgement:

Part of this work (DS) was supported by NASA contract 704-40-32 to CSC at NASA's Ames Research center. KC and CW acknowledge a support from NASA contract NCC2-5400-2. KC acknowledges many helpful discussions with Dr. M. Baskes and Prof. R. Ruoff on nanotube mechanics.

REFERENCES:

[1] S. Iijima, Nature (London) **354**, 56 (1991)
[2] S. Iijima, and T. Ichihashi, Nature, **363**, 603 (1993)

[3] D.S. Bethune et al, Nature **363**, 605 (1993)
[4] R. Saito, G. Dresselhaus, and M.S. Dresselhaus, "*Physical Properties of Carbon Nanotubes*", Imperial College Press (1998)
[5] M.S. Dresselhouse, G. Dresselhaus, and Ph. Avouris (Eds.), "*Carbon Nanotubes: Synthesis, Structure, Properties, and Applications*" Springer-Verlag Berlin Heidelberg (2001)
[6] D.W. Brenner, O.A. Shenderova and D.A. Areshkin, "*Reviews in Computational Chemistry*, K.B. Lipkowitz and D.B. Boyd, Eds., 213 (VCH Publishers, New York, 1998) and references there in.
[7] B. J. Garrison and D. Srivastava, Ann. Rev. Phys. Chem. **46**, 373 (1995) and references there in.
[8] M. P. Allen and D. J. Tildsley, *Computer Simulations of Liquids*, (Oxford: Oxford Science Publications 1987
[9] D. Srivastava and S. Barnard, Proc. IEEE Supercomputing **97** (SC '97 cd-rom) (1997)
[10] W. A. Harrison, *Electronic Structure and the Properties of Solids*, (Freeman, San Francisco, 1980)
[11] M. Menon and K.R. Subbaswamy, Phys. Rev. **B55**, 9231 (1997)
[12] M. Menon, J. Chem. Phys. **114**, 7731 (2000)
[13] Payne et al., Rev. Mod. Phys. **68**, 1045 (1992) for a detailed review
[14] P. Hohenberg and W. Kohn, Phys. Rev. **136**, B864 (1964)
[15] W. Kohn and L.J. Sham, Phys. Rev. **140**, A1133 (1965)
[16] Check the web site for the details, http://cms.mpi.univie.ac.at/vasp/
[17] D. Srivastava, M. Menon and K. Cho, "Computational Nanotechnology with Carbon Nanotubes and Fullerenes," *Computing in Engineering and Sciences*, special issue on Nanotechnology, page 42, July/Aug (2001)
[18] D.H. Robertson, D.W. Brenner, and J.W. Mintmire, Phys. Rev. B **45**, 12592 (1992)
[19] G.G. Tibbetts, J. Cryst. Growth **66**, 632 (1983)
[20] J.P. Lu, Phys. Rev. Lett. **79**, 1297 (1997)
[21] E. Hernandez, C. Goze, P. Bernier, and A. Rubio, Phys. Rev. Lett. **80**, 4502 (1998)
[22] B.I. Yakobson, C.J. Brabec, and J. Bernholc, Phys. Rev. Lett. **76**, 2511-2514 (1996)
[23] D. Sanchez-Portal et al, Phys. Rev. **B59**, 12678 (1999)
[24] D. Srivastava, M. Menon, and K. Cho, Phys. Rev. B **63**, 195413 (2001)
[25] L.D. Landau and E.M. Lifschitz, "*Theory of elascity*", 2nd ed. Oxford (1975)
[26] P. Poncharal et al, Science **283**, 1513 (1999)
[27] S. Iijima et al, J. Chem. Phys. **104**, 2089 (1996)
[28] M.M.J. Treacy, T.W. Ebbesen, and J.M. Gibson, *Nature* **381**, 678 (1996)
[29] E.W. Wong, P.E. Sheehan, and C.M. Lieber, Science **277**, 1971 (1997)
[30] A. Krishnan, E. Dujardin, T.W. Ebbesen et al, Phys. Rev. B **58**, 14013 (1998)
[31] J.P. Salvetat et al, Phys. Rev. Lett. **82**, 944 (1999)
[32] O. Lourie, D.M. Cox, and H.D. Wagner, Phys. Rev. Lett. **81**, 1638 (1998)
[33] D. Srivastava, M. Menon, K. Cho, Phys. Rev. Lett. **83**, 2973 (1999)
[34] M.B. Nardelli, B.I. Yakobson, and J. Bernholc, Phys. Rev. Lett. **81**, 4656 (1998); M.B. Nardelli, B.I. Yakobson, and J. Bernholc, Phys. Rev. B **57**, 4277 (1998)
[35] P. Zhang et al, Phys. Rev. Lett. **81**, 5346 (1998)
[36] B.I. Yakobson, M.P. Campbell, C.J. Brabec, and J. Bernholc, Comput. Mater. Sci. **8**, 341 (1997)
[37] D.A. Walters et al, Appl. Phys. Lett. **74**, 3803 (1999)
[38] M.F. Yu et al, Phys. Rev. Lett. **84**, 5552 (2000)
[39] M.F. Yu et al, Science **287**, 637 (2000)
[40] C. Wei, K. Cho, and D. Srivastava, submitted (2002)
[41] C. Wei, D. Srivastava, and K. Cho, to appear, *Computer Modeling in Engineering and Sciences* (2001)
[42] B. Vigolo et al, Science, **290**, 1331 (2000)
[43] L.S. Schadler, S.C. Giannaris, and Ajayan PM, Appl. Phys. Lett.**73**, 3842 (1998)
[44] R. Andrews et al, Appl. Phys. Lett. **75**, 1329 (1999)
[45] M.A. Osman, and D. Srivastava, Nanotechnology **12**, 21 (2001)
[46] C. Wei, D. Srivastva, and K. Cho, submitted (2001)
[47] S.J.V. Frankland, A. Caglar, D.W. Brenner, and M. Griebel, MRS Symposium Proceedings, **A14**.17 Fall (2000)
[48] H.D. Wagner, O. Lourie, Y. Feldman, and R. Tenne, Appl. Phys. Lett.**72**, 188 (1998)
[49] O. Lourier and H.D. Wagner, Appl. Phys. Lett. **73**, 3527 (1998)
[50] Q. Qian, E.C. Dickey, R. Andrews, and T. Rantell, Appl. Phys. Lett.**76**, 2868 (2000)

FIGURE CAPTIONS:

Figure 1. (a) A graphene sheet made of C atoms placed at the corners of hexagons forming the lattice with arrows AA and ZZ denoting the rolling direction of the sheet to make (b) an (5,5) armchair and (c) a (10,0) zigzag nanotubes, respectively.

Figure 2. Young's modulus as a function of the tube diameter for C, BN, BC_3, BC_2N from tight binding simulation. (From Hernandez et al, *PRL*, **80**, 4502, 1998)

Figure 3. Young's modulus verse tube diameter for ab initio simulation. Open symbols for the multiwall CNT geometry and solid symbols for the single wall tube with crystalline-rope configuration. The experimental value of the elastic modulus of graphite is also shown. (From Sanchez-Portal et al, *PRB* **59**, 12678, 1999)

Figure 4. Bending stiffness as a function of tube diameter from MD simulation with Tersoff-Brenner potential. The stiffness is scaled as $D^{2.93}$, closed to the cubic dependence on diameter D predicted from continuum elastic theory.

Figure 5. (a) Bending modulus as a function of tube diameter. Solid circles are from Poncharal et al (*Science* **283**, 1513, 1999);others are from other experiments as referred in Poncharal et al's paper. The dropping in the bending modulus is attributed to the onset of a wavelike distortion in lateral direction as shown in (b). **(b).** High –resolution TEM image of a bent nanotube (Radius of curvature ≈ 400nm), showing the wavelike distortion and the magnified views. (From Poncharal et al, *Science* 283, 1513, 1999)

Figure 6. HREM images of kink structures formed in bent CNTs. Shown on left is a single kink in a SWCNT with diameter 1.2nm; Shown on tight is a kink on a MWCNT with diameter 8 nm. (From Iijima et al, *J. Chem. Phys.* **104**, 2089, 1996)

Figure 7. The torsion stiffness as a function of tube diameter for a series of zigzag and armchair SWNTs calculated with Tersoff-Brenner potential. The stiffness is scaled as $D^{3.01}$ for D>0.8nm, in agree with the prediction from continuum elastic theory.

Figure 8. (a) The strain energy of a compressed 6nm long (7,7) CNT, from Tersoff-Brenner potential, has four singularities corresponding to the buckled structures with shapes shown in (b) to (e). The CNT is elastic up to 15% compression strain despite of the highly deformed structures. The MD study was conducted at T = 0K. (From Yakobson et al, *PRL*, **76** 2511, 1996)

Figure 9. TEM image of fractured multiwalled carbon nanotubes under compression within a polymeric film. The enlarged image is shown on right. (From Wagner et al, *PRL*, 81 1628, 1998)

Figure 10. Shown on right from (a) to (d) are four stages of spontaneous plastic collapse of the 12% compressed (8,0) CNT, with diamond like structures formed at the location of the collapse. (From Srivastava el al, *PRL*, **83** 2973, 1999)

Figure 11. Five stages of spontaneous plastic collapse of the 14.25% compressed (8,0) BN nanotube. (a) Nucleation of deformations near the two ends, (b)-(d) anisotropic strain release in the central compressed section and plastic buckling near the right end of the tube, and (e) the final anisotropically buckled structure where all the deformation is transferred toward the right end of the tube. The cross section of each structure is shown on right.

Figure 12. The Stone Wales bond rotation on a zigzag and an armchair CNT, resulting pentagon-heptagon pairs, can lengthen a nanotube, with the greatest lengthening for an armchair tube. (From Zhang et al, *PRL* **81**, 5346, 1998)

Figure 13. A heptagon-pentagon pair appeared on a 10% tensile strain (10,10) CNT at T = 2000K. Plastic flow behavior of the Pentagon-heptagon pairs after 2.5ns at T=3000K on a 3% tensile strained CNT. The shaded region indicates the migration path of the (5-7) edge dislocation. (From Nardelli et al, *PRL* **81** 4656, 1998)

Figure 14. Left: Eight stress versus strain curves obtained from the tensile-loading experiments on individual SWCNT ropes. The Young's modulus is ranged from 320GPa to 1470 GPa. The breaking strain was found at 5.3% or lower. (From Yu et al, *PRL* **84** 5552, 2000) Right: Plot of stress versus strain curves for individual MWCNTs. The Young's modulus is ranged form 270GPa to 950 GPa, with breaking strain around 12% (one sample showed a 3% breaking strain). (From Yu et al, *Science* **287** 637, 2000)

Figure 15. The yielding strain of a 6nm long (10,0) CNT is plotted as functions of strain rate and temperature. Stone-Wales bond rotations appear first resulting in heptagon and pentagon ring; then larger C rings generated around such defects followed by the necking of the CNT; and the CNT is broken shortly after. (From MD simulations with Tersoff-Brenner potential)

Figure 16. Left: A 9% tensile strained (5,5) CNT with numerous Stone-Wales bond rotation defects at 2400K, and the following breaking of the tube. Right: An 11.5% tensile strained (10,0) with a group of pentagon and heptagon centered by an octagon at 1600K, and the following breaking of the tube. (From MD simulation with Tersoff-Brenner potential)

Figure 17. A 12% compressed (10,0) CNT at T=1600K. A Stone-Wales dislocation defect can be seen at the upper section of the CNT. Several sp3 bonds formed in the buckled region. (From MD simulation with Tersoff-Brenner potential)

Figure 18. Density as a function of temperature for a polyethylene system (50 chains with $Np = 10$), and a CNT-polyethylene composite (2nm long capped (10,0) CNT) The CNT composite has an increase of thermal expansion above T_g. (From a MD simulation with Van der Waals potential between CNT and matrix. Dihedral angle potential and torsion potential were used for the polyethylene matrix, and Tersoff-Brenner potential was used for carbon atom on the CNT)

Figure 19. Plot of the stress versus strain curve for pure polyethylene matrix and CNT composite (8 vol. %) at small strain region (T = 50K). Young's modulus is increased 30% for the composite. (From MD simulation)

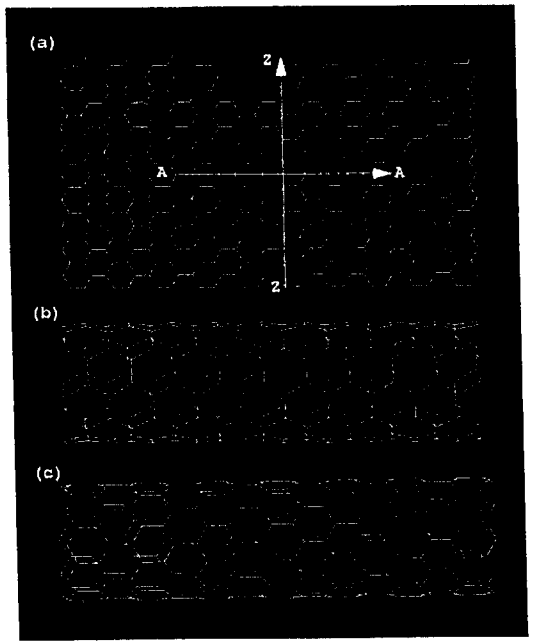
(a)
z
A
A
z
(b)
(c)

Fig 1

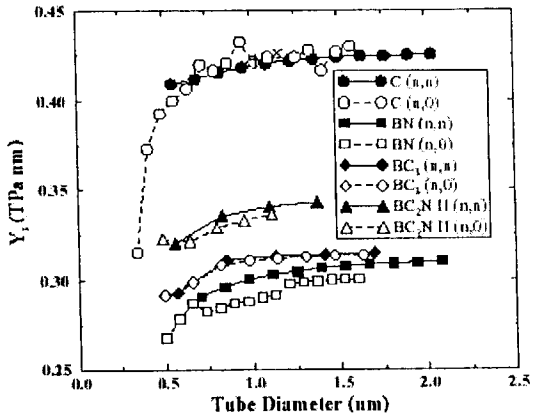
0.45
0.40
0.35
0.30
0.25
0.0
0.5
1.0
1.5
2.0
2.5
Y, (TPa nm)
Tube Diameter (nm)
C (n,n)
C (n,0)
BN (n,n)
BN (n,0)
BC3 (n,n)
BC3 (n,0)
BC2N II (n,n)
BC2N II (n,0)

Fig 2

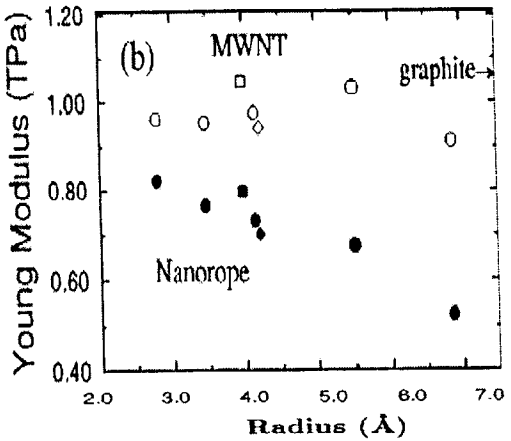
(b)
MWNT
graphite
Nanorope
Young Modulus (TPa)
1.20
1.00
0.80
0.60
0.40
2.0
3.0
4.0
5.0
6.0
7.0
Radius (Å)

Fig 3

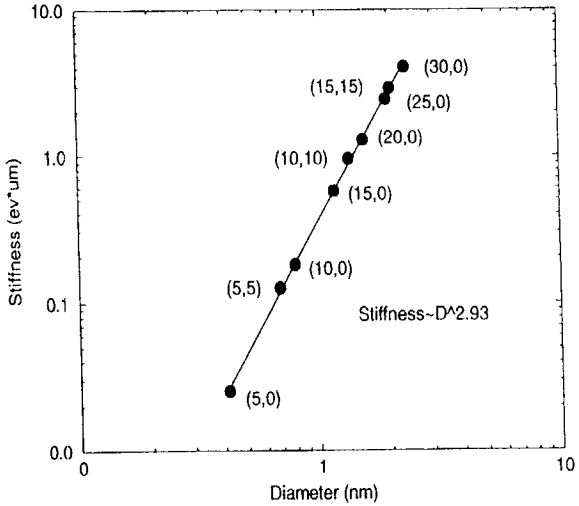
10.0
1.0
0.1
0.0
Stiffness (ev*um)
0
1
10
Diameter (nm)
(30,0)
(15,15)
(25,0)
(20,0)
(10,10)
(15,0)
(10,0)
(5,5)
(5,0)
Stiffness~D^2.93

Fig 4

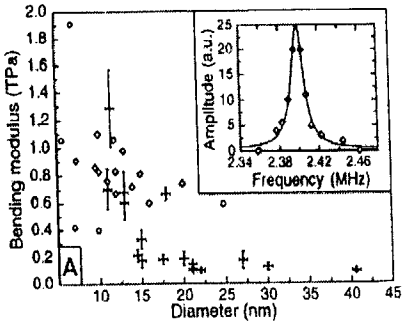

Fig 5 (a)

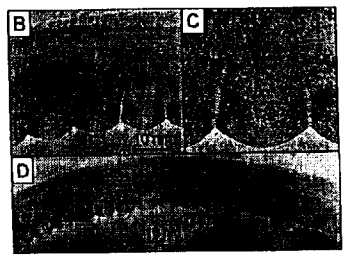

Fig 5 (b)

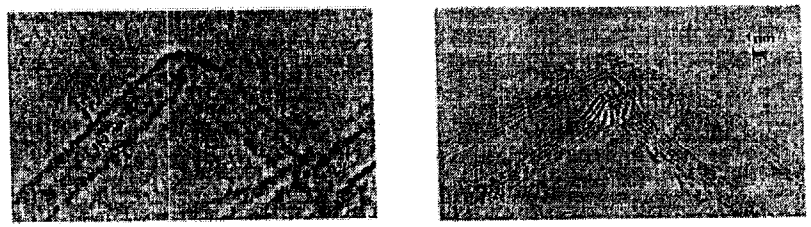

Fig 6

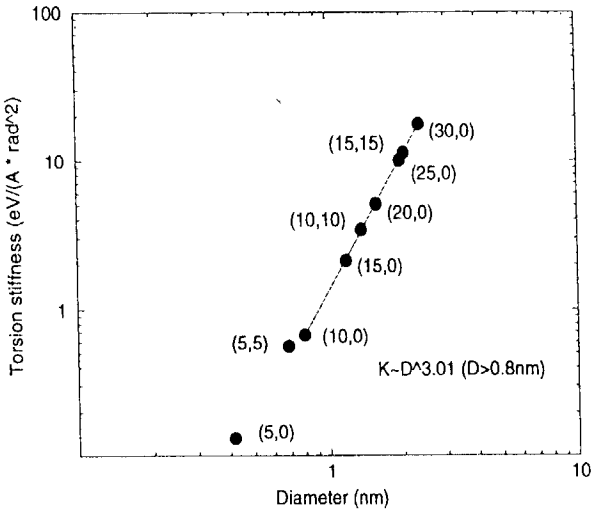

Fig 7

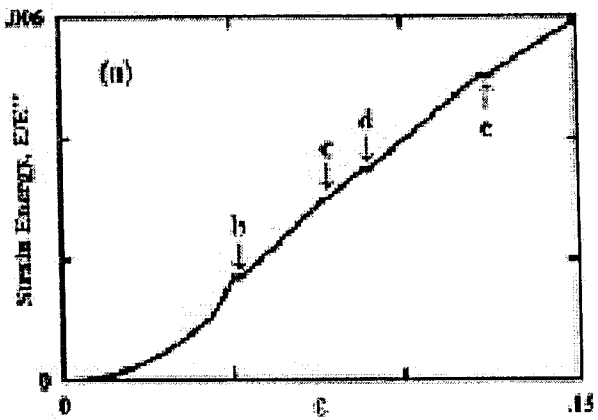

Fig 8 (a)

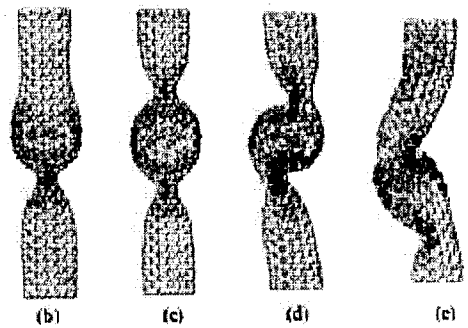

Fig 8 (b)

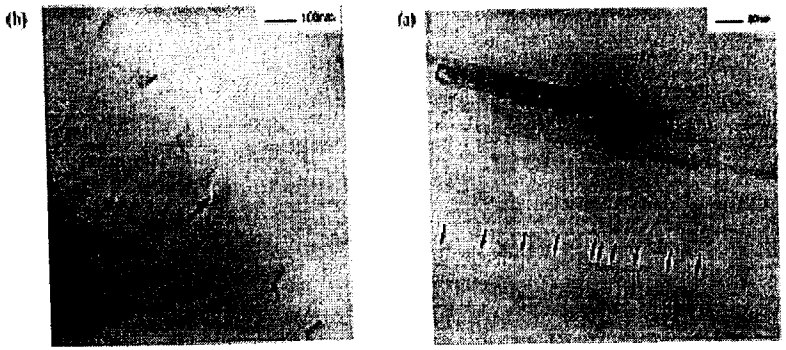
(b)
(d)

Fig 9

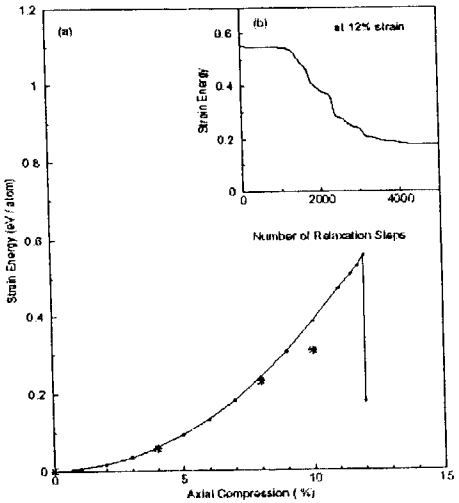
(a)
(b)
at 12% strain
Strain Energy
Number of Relaxation Steps
Strain Energy (eV / atom)
Axial Compression (%)

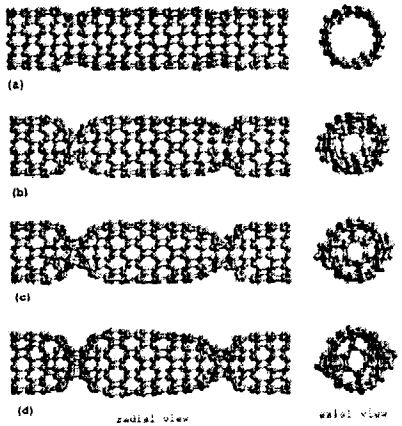
(a)
(b)
(c)
(d)

Fig 10

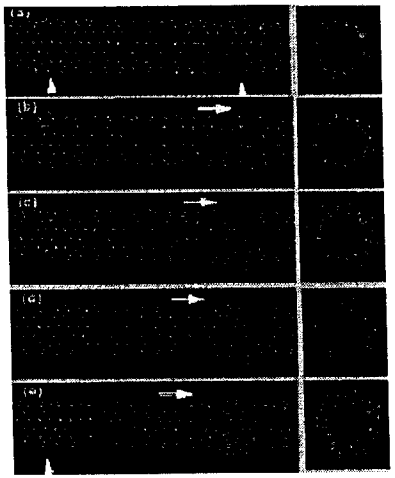

Fig 11

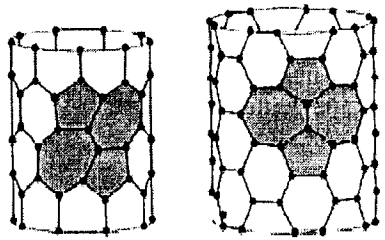

Fig 12

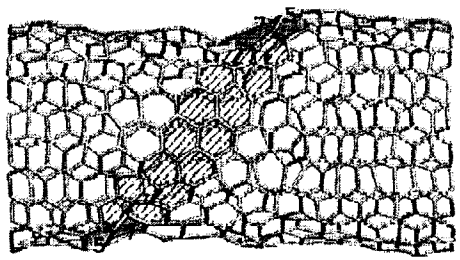

Fig 13

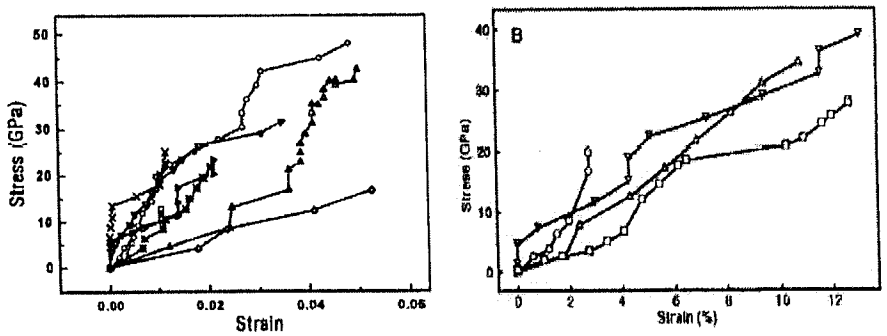

Fig 14

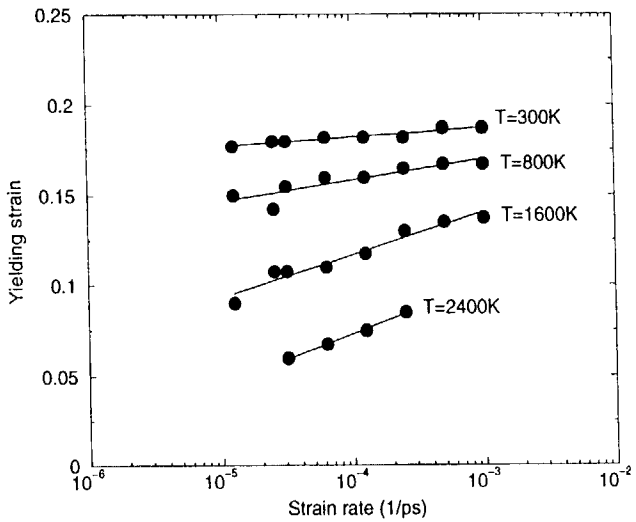
0.25
0.2
0.15
0.1
0.05
0
Yielding strain
T=300K
T=800K
T=1600K
T=2400K
10^{-6}
10^{-5}
10^{-4}
10^{-3}
10^{-2}
Strain rate (1/ps)

Fig 15

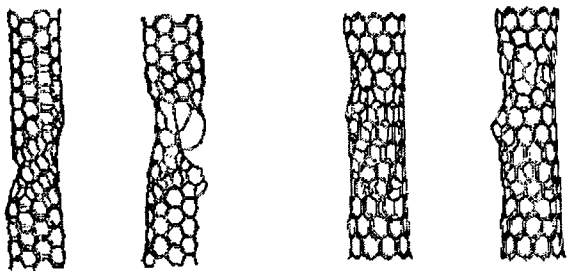

Fig 16

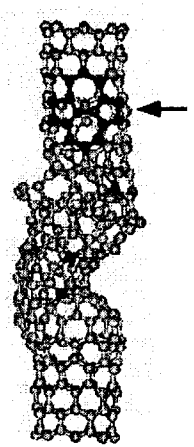

Fig 17

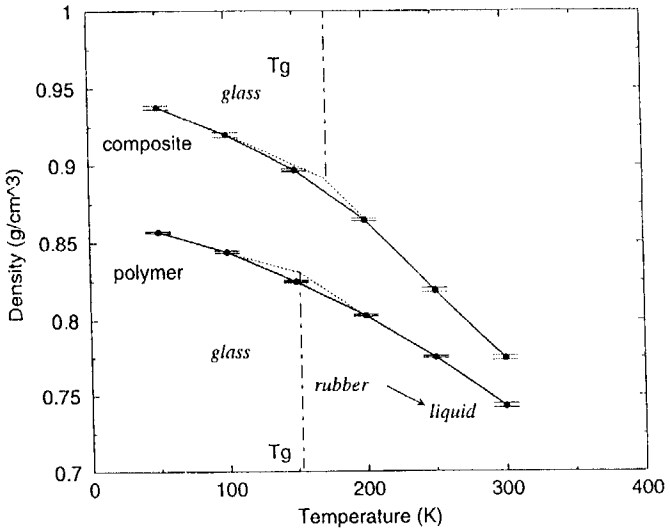
1
0.95
0.9
0.85
0.8
0.75
0.7
Density (g/cm^3)
0
100
200
300
400
Temperature (K)
Tg
glass
composite
polymer
glass
rubber
liquid
Tg

Fig 18

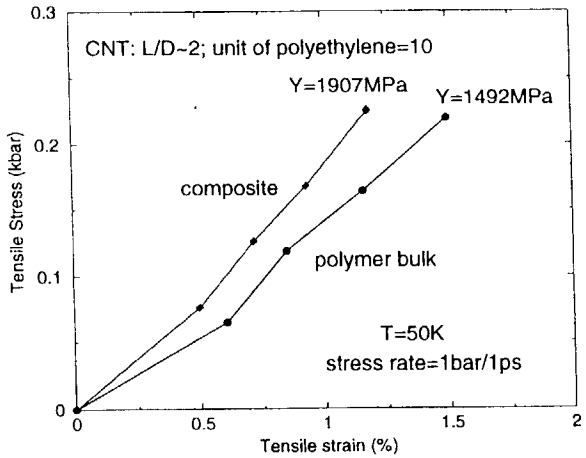
CNT: L/D~2; unit of polyethylene=10
Y=1907MPa
Y=1492MPa
composite
polymer bulk
T=50K
stress rate=1bar/1ps
Tensile Stress (kbar)
Tensile strain (%)
0.3
0.2
0.1
0
0
0.5
1
1.5
2

Fig 19